Low complexity OSNR monitoring and modulation format identification based on binarized neural networks

Yilun Zhao, Zhenming Yu, Zhiquan Wan, Shaohua Hu, Liang Shu, Jing Zhang, and Kun Xu, *Member, IEEE*

***Abstract*—We propose and experimentally demonstrate a method of optical signal-to-noise ratio (OSNR) monitoring and modulation format identification (MFI) using a binarized convolutional neural network (B-CNN) in coherent receiver. The proposed technique automatically extracts OSNR and modulation format dependent features from the signals' ring constellation maps. A group of modulation schemes including nine quadrature amplitude modulation (QAM) formats are selected as transmission signals. The experimental results show that the MFI accuracy can reach 100% and OSNR monitoring accuracy can reach higher than 97.71% for the nine M-QAM modulation formats. Compared with float valued convolutional neural network (F-CNN) and multi-layer perceptron (MLP), B-CNN can reach the same performance in MFI. For OSNR monitoring, the performance of B-CNN is similar to MLP and slightly worse than F-CNN. Moreover, the memory consumption and execution time of B-CNN is much lower than F-CNN and MLP. Therefore, B-CNN is power and time efficient with little performance loss compared with F-CNN and MLP. It is attractive for cost-effective multi-parameter estimation in next-generation optical networks.**

***Index Terms*—Modulation format identification (MFI), OSNR monitoring, binarized neural networks (BNNs), optical fiber communications.**

I. Introduction

WITH the increasing of the demand for simultaneously supporting various data services, optical network is evolving from current fixed architecture to future flexible and elastic one [1]–[5]. Since different services and users require specific quality of service (QoS), the network environment becomes heterogeneous and requires complex management by human administrators and technicians. To realize flexible network management and reduce human intervention, it is desirable to develop a cognitive optical network (CON) [6]–[9]. The aim of CON is to introduce intelligence into the control plane that allows for autonomous end-to-end performance optimization and minimization of required human intervention. A CON is also capable of coordinating transmitters and receivers for real-time dynamic adjustment of the modulation format, line rate, spectrum allocation and other parameters. Managing the transceivers in this way could help to realize intelligent channel management, bandwidth allocation and other link functions at the network nodes, thereby improving service quality and transmission quality. In order to reduce operating costs, ensure optimum resources utilization and guarantee adequate operation and management of CON, it is essential to continuously monitor various network performance parameters, which is referred to as optical performance monitoring (OPM) [10]–[13]. Since most of the linear impairments can be fully compensated, transmission performance is largely determined by the optical signal-to-noise-ratio (OSNR) and hence OSNR estimation is especially vital for coherent links. Moreover, the OSNR monitoring technique must be appropriate for the incoming signal type, and the carrier recovery module used in the receiver must be suitable for the received modulation format. Therefore, modulation format identification (MFI) is also indispensable for digital receivers in CON.

Recently, machine learning techniques, especially deep neural networks (DNNs), have achieved significant progress in various areas. Many researches have employed DNN in optical communication system to solve various problems [14]–[25]. Traditional OPM methods can only implement one of MFI [26]–[29] and OSNR monitoring [30]–[33] and require substantial prior expertise. On the contrary, DNN-assisted methods [18]–[25] can simultaneously perform MFI and OSNR monitoring from raw data. The capacity of DNN to monitor multiple parameters simultaneously is essential for OPM, since a CON must depend on real-time information about various parameters from physical layer to make future prediction and decision. Previous DNN-assisted OPM methods widely explored different architectures of DNNs, including the architecture consisted of multiple networks and each was responsible for a different task [18], [21], and one single network using multi-task learning framework [20], [22], [23], [25]. In addition, different features and network types are also investigated. Amplitude histograms (AHs) [18], [22], [23], [25], constellation diagrams [19], [21], and asynchronous delay-tap plots (ADTPs) [20], [24] were chosen as input features to fully-connected DNN, also called multi-layer perceptron (MLP) [18], [22], [25] and convolutional neural network

This work was supported in part by the NSFC Program (No. 61821001, 61625104, 61901045); National Key R&D Program of China (No. 2018YFB2201803, 2019YFB1803504); Fundamental Research Funds for the Central Universities(No. 2019RC11); the Fund of State Key Laboratory of Information Photonics and Optical Communication BUPT (No. IPOC2017ZT08). (*Corresponding author: Zhenming Yu*)

Y. Zhao, Z. Yu, Z. Wan, L. Shu, and K. Xu are with the State Key Laboratory of Information Photonics and Optical Communications, Beijing University of Posts and Telecommunications, Beijing, 100876, China (e-mail: zyl2018111137@bupt.edu.cn; yuzhenming@bupt.edu.cn; wanzhiquan@bupt.edu.cn; shuliang@bupt.edu.cn; xukun@bupt.edu.cn).

S. Hu and J. Zhang, was with Key Laboratory of Optical Fiber Sensing and Communications, University of Electronic Science and Technology of China, Chengdu, 611731, China (email:hshhfmy@std.uestc.edu.cn; zhangjing1983@uestc.edu.cn).

(CNN) [19], [23], [24]. Previous schemes, either in single-task or multi-task framework, employed float-valued DNNs, either CNN or MLP. However, DNNs are almost exclusively trained and run on one or many very fast and power-hungry graphic processing units (GPUs) [34]. As a result, it is a challenge to deploy DNN in optical communication system. To be more specific, there are many digital signal processing (DSP) modules in a coherent receiver, such as adaptive equalization and carrier phase recovery that require real-time information about current modulation format. Therefore, a flexible digital coherent receiver will have strict latency requirement for OPM, while the large-scale float valued operations of DNNs are time consuming. Moreover, the memory resources are limited in real-time DSP circuits, while DNNs usually take up a lot of memory. All these factors make it unpractical to integrate DNN into coherent receivers. Although we could use external devices to perform OPM, this method will increase the total cost a lot and the communication latency between receivers and OPM devices is also unacceptable. In conclusion, it is significant to reduce the complexity of DNN to perform intelligent OPM in future CON.

In this paper, we propose a novel intelligent optical performance monitoring technique. We choose the constellation diagrams after constant modulus algorithm (CMA) as input features and then perform joint MFI and OSNR monitoring using a binarized convolutional neural network (B-CNN), which can reach high accuracies of joint MFI and OSNR monitoring with low memory consumptions and computational complexity. The B-CNN is constructed based on binarized neural networks (BNNs) [35] with binary weights and activations at run-time during the forward pass, BNNs drastically reduce memory size and accesses, and is expected to substantially improve power-efficiency. To verify the proposed method, we set up a 12.5 Gbaud flexible dual-polarization (DP) quadrature amplitude modulation (QAM) system with transmission of 5 km standard single mode fiber (SSMF). We first investigate how resolution and sample length of a grayscale map influence the performance of the proposed method. Then we compare the performance of B-CNN with float-valued CNN (F-CNN) and MLP. The experimental results show that B-CNN can reach similar performance with the other two DNNs, while B-CNN has the lowest memory consumption and fastest execution speed at run-time. In addition, we further evaluate the robustness of proposed method in simulation.

The rest part of the paper are structured as follows: Section II introduces the main operating principle behind this work. In this section, we first describe how to train and optimize a BNN, then we describe our modulation scheme and the method that we use to prepare data for training. Section III details the experimental system of OPM and the model structure of B-CNN. Section IV reports the performance of our system and the comparison between B-CNN, F-CNN and MLP. Section V further discusses robustness of DNN-assisted methods in a system with dynamic parameters and Section VI concludes the work.

II. Operating principle

A. Binarized neural networks

When training a BNN, both the weights and the activations are constrained to either +1 or -1. We select a deterministic function to transform the real-valued variables into those two values:

$$x^b = \mathrm{Sign}(x) = \begin{cases} +1 & \text{if } x \geq 0, \\ -1 & \text{otherwise}, \end{cases} \tag{1}$$

where x^b is the binarized variable (weight or activation) and x is the real-valued variable. Since the derivative of the sign function is zero almost everywhere, making it apparently incompatible with back-propagation, an approach called straight-through estimator is adopted [35]. Here we denote an input of a neuron by r and the corresponding output of the neuron by q. Thus q is computed by *sign* function quantization

$$q = \mathrm{Sign}(r). \tag{2}$$

When performing back-propagation, we denote the loss function by C. According to the chain rule, we can compute the gradient $\partial C/\partial r$ by

$$\frac{\partial C}{\partial r} = \frac{\partial C}{\partial q} \times \frac{\partial q}{\partial r}. \tag{3}$$

Assume that an estimation g_q of the gradient $\partial C/\partial q$ has been obtained (with the straight-through estimator when needed). Since the derivative of *sign* function is zero, we estimate the derivative $\partial q/\partial r$ by assuming that

$$\frac{\partial q}{\partial r} = \begin{cases} 1 & \text{if } |x| \leq 1, \\ 0 & \text{otherwise}. \end{cases} \tag{4}$$

Then we can compute the estimation g_r of the gradient $\partial C/\partial r$ by

$$g_r = g_q \times 1_{|r|\leq 1}. \tag{5}$$

Where $1_{|r|\leq 1}$ denote $\partial q/\partial r$ in a straight-through estimator. Note that this preserves the gradient's information and cancels the gradient when r is too large. To be more specific, when the input is either larger than 1 or smaller than -1, we cancel its gradient and do not update its value anymore, otherwise we assume the gradient is 1 and spread it in the back-propagation process. The use of this straight-through estimator can also be seen as propagating the gradient through *hard-tanh*, which is the following piece-wise linear activation function:

$$\mathrm{Htanh}(x) = \mathrm{Clip}(x, -1, 1) = \max(-1, \min(1, x)). \tag{6}$$

Based on the above method, we can update the real-valued weight w^r during training time. When the weight update bring w^r outside of $[-1, 1]$, we project w^r to -1 or 1. Otherwise, the real-valued weights would grow very large without any impact on the binary weights. When using a weight w^r, we quantize it using $w^b = \mathrm{Sign}(w^r)$. Therefore the real-valued weights do not participate in forward propagation of a network.

This article has been accepted for publication in a future issue of this journal, but has not been fully edited. Content may change prior to final publication. Citation information: DOI 10.1109/JLT.2020.2973232, Journal of Lightwave Technology

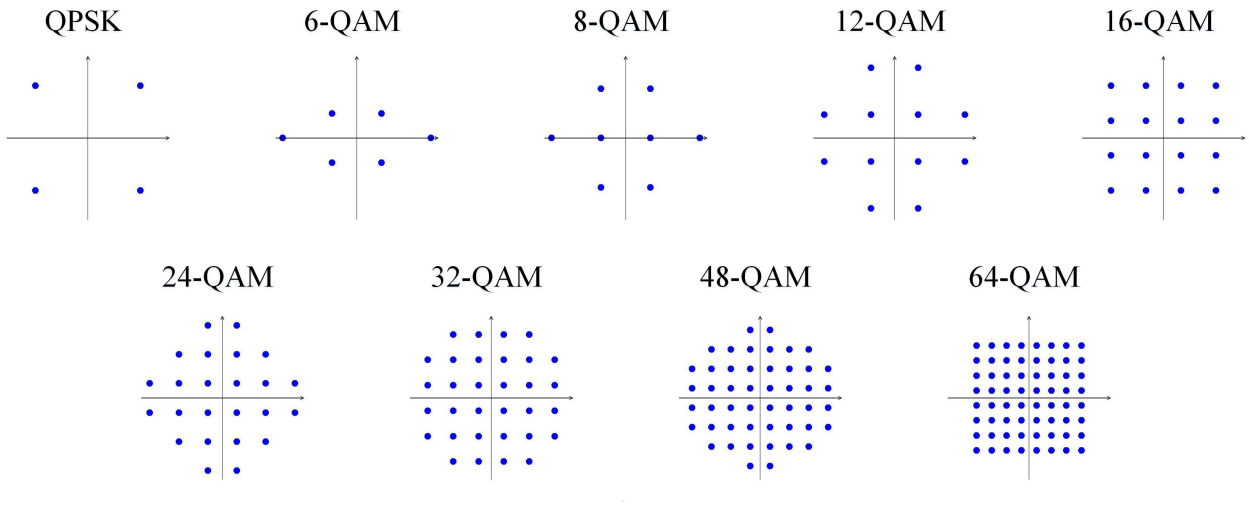

Fig. 1. Nine schematic constellation diagrams of modulation format adaptive M-QAM scheme.

For classification tasks, *cross-entropy* loss is commonly used to measure the performance of a model whose output is a probability between 0 and 1. It is calculated as

$$-\sum_{c=1}^{M} y_{o,c}\log(p_{o,c}), \tag{7}$$

where M is the number of classes, $y_{o,c}$ is a binary indicator (0 or 1) if class label c is correct classification for observation o and $p_{o,c}$ is the predicted probability observation o is of class c. The predicted probability $p_{o,c}$ is calculated by using *softmax* as activation function in the output layer. The *softmax* function is defined by Eq. (8), where $(z_1,\ldots,z_M)$ is the output vector of output layer.

$$p_{o,c} = \frac{e^{z_c}}{\sum_{k=1}^{M} e^{z_k}}, \text{for } c = 1,\ldots,M \tag{8}$$

For BNNs, since all the activation functions are replaced with *hard-tanh* in training stage and *sign* function is adopted in running stage, there exist negative values in the output of last layer i.e. the output is not a probability between 0 and 1. As a result, the *cross-entropy* loss fail to work. Therefore, we choose *squared-hinge* function as the loss function given by Eq. (9), where y is the output of a neuron and t is the target value.

$$L(y,t) = \max\left(0,(1-yt)^2\right) \tag{9}$$

B. Modulation scheme and data preparation

Adaptive modulation increase the capacity of network by adjusting the modulation formats according to current channel status. In coherent system, QPSK, 16-QAM and 64-QAM are the most popular modulation formats. However, the gap between these three modulation formats is too large. In [36], a group of modulation schemes of M-QAM are proposed to improve the capacity of flexible bandwidth adjustment. Fig. 1 shows the constellation points of the proposed nine modulation format adaptive M-QAM. After in-phase (I) quadrature (Q) imbalance compensation, chromatic dispersion (CD) compensation and CMA equalization, the grayscale maps at X-polarization with phase rotation are shown in Fig. 2. In order to reduce the computation load and enhance the ability to express the characteristics of different modulation formats, we directly generate the grayscale maps of constellation diagrams instead of first collect colored constellation diagrams [19], [24] because the grayscale map has only one channel. The value of the pixel represents the density of the constellation points of the corresponding grid.

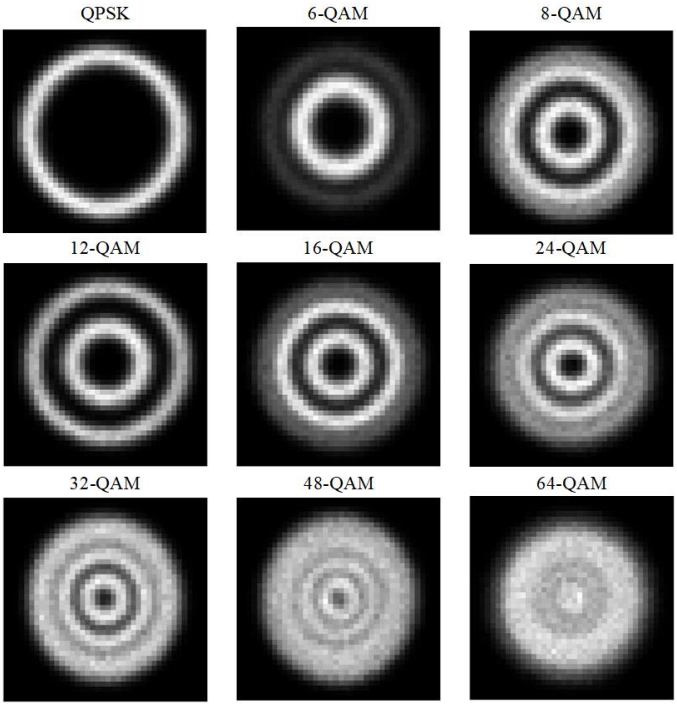

Fig. 2. The grayscale map of each modulation format at OSNR of 25 dB.

Based on the above scheme, we randomly generate 5 groups of 4×10^6 symbols at the transmitter. For each group of symbols, we collect 20 grayscale maps from 20 time periods

This article has been accepted for publication in a future issue of this journal, but has not been fully edited. Content may change prior to final publication. Citation information: DOI 10.1109/JLT.2020.2973232, Journal of Lightwave Technology

without overlap at the receiver. As a result, 100 different grayscale images for each OSNR value of each modulation format are collected as data set. More specifically, each format has 1600 grayscale maps for 16 OSNR values ($10 \sim 25$ dB for QPSK, 6-QAM, 8-QAM, 12-QAM, $15 \sim 30$ dB for 16-QAM, 24-QAM, and $20 \sim 35$ dB for 32-QAM, 48-QAM, and 64-QAM). Therefore, the data set consists of $100 \times 16 \times 9 = 14400$ samples in total. Then we randomly mess up the data set and take 50% as train set, 25% as validation set and the other 25% as test set. In the training set, each map has a label vector. In CNN, the label vector is composed of several binary bits, the amount of binary bits is equal to the class number. In our scheme, since all the weights and neurons are binarized and constrained to +1 and -1, the elements of the label vector are either +1 or -1. We set the first 9 bits to denote the modulation formats, and the other 16 bits to denote the 16 OSNR values. Thus the output label vector consists of 25 bits totally. Table I illustrates the relationship between modulation formats and corresponding label vectors by listing the labels of QPSK, 16-QAM, and 64-QAM signals.

TABLE I
EXAMPLES OF LABEL VECTORS

Signal type	Label vector
QPSK, 10 dB	$\underbrace{+1-1\cdots-1}_{9}\underbrace{+1-1\cdots-1}_{16}$
QPSK, 11 dB	$\underbrace{+1-1\cdots-1}_{9}\underbrace{-1+1\cdots-1}_{16}$
QPSK, 25 dB	$\underbrace{+1-1\cdots-1}_{9}\underbrace{-1\cdots-1+1}_{16}$
16-QAM, 15 dB	$\underbrace{-1\cdots+1\cdots-1}_{9}\underbrace{+1-1\cdots-1}_{16}$
16-QAM, 16 dB	$\underbrace{-1\cdots+1\cdots-1}_{9}\underbrace{-1+1\cdots-1}_{16}$
16-QAM, 30 dB	$\underbrace{-1\cdots+1\cdots-1}_{9}\underbrace{-1\cdots-1+1}_{16}$
64-QAM, 20 dB	$\underbrace{-1-1\cdots+1}_{9}\underbrace{+1-1\cdots-1}_{16}$
64-QAM, 21 dB	$\underbrace{-1-1\cdots+1}_{9}\underbrace{-1+1\cdots-1}_{16}$
64-QAM, 35 dB	$\underbrace{-1-1\cdots+1}_{9}\underbrace{-1\cdots-1+1}_{16}$

III. SYSTEM SETUP AND NETWORK STRUCTURES

A. Optical communication system

The experimental setup for the demonstration of the proposed OSNR monitoring and MFI technique is shown in Fig. 3. We generate 12.5 Gbaud M-QAM optical signals by modulating a carrier signal, provided by an external cavity laser (ECL), using I/Q modulators which are driven by multi-level electrical signals. The center wavelength of ECL is 1552.52 nm and its linewidth is 100 kHz. Polarization multiplexing is then realized by utilizing polarization beam splitters (PBSs), polarization beam combiners (PBCs), and optical delay lines. The resulting signals are amplified using an erbium-doped fiber amplifier (EDFA) and sent over a 5 km long SSMF. A variable optical attenuator (VOA) is utilized to alter OSNRs of M-QAM signals. The optical signals at the output of EDFA are filtered using a 0.6 nm optical band-pass filter (OBPF) and then detected by a coherent receiver. The electrical signals after optical-to-electronic (O/E) conversion are sampled by utilizing an oscilloscope with 50 Gsamples/s sampling rate and 1.6×10^7 samples are collected, which are then processed offline using a DSP core. As clear from Fig. 3, the proposed technique processes polarization de-multiplexed signals after CMA equalization. We generate grayscale constellation maps directly from the signals and input to the B-CNN for joint MFI and OSNR monitoring. Finally, the modulation format information is used to conduct multiple modulo algorithm (MMA)-based equalization, carrier phase recovery and symbol detection & decision, and the OSNR information is utilized to perform fault & link health detection to assist the cognitive management in a CON.

B. Network structures of DNNs

We build up the neural network model based on [37]. The network structure of B-CNN is displayed in Fig. 3, which consists of 2 convolutional layers, 1 maxpooling layer and 2 fully-connected (FC) layers. The first layer has 64 filters (convolution kernels) and the second layer has 128 filters. All the filters have the same size of 4×4. Then the 2 convolutional layers are followed by a 2×2 maxpooling layer to reduce parameters size. Finally, the three-dimensional data is flattened and then processed by 2 FC layers and the first FC layer has 512 neuron nodes. The second FC layer has 25 nodes, which are equal to the number of elements of target label vectors. As a comparison, a F-CNN with the similar architecture to B-CNN and a MLP with four FC layers are adopted. In the F-CNN, the filter numbers for the two convolutional layers are 32 and 64 respectively, the filter size is 3×3. The first FC layer of F-CNN contains 128 neuron nodes and the second FC layer has 25 nodes. In the MLP, the first and third layers contain 1024 neuron nodes, the second layer contains 2048 neurons nodes, and the ourput layer contains 25 nodes. In F-CNN and MLP, *sigmoid* is selected as activation function of output layer and *relu* is selected as activation function of other hidden layers. *Sigmoid* and *relu* are defined by Eq. 10,11 respectively, where y is the output of activation and x is the input. For all DNNs, *Adam* optimizer is adopted because it is computationally efficient and requires less memory [38]. Besides, we adopt *Batchnormalization* between each layer by performing the normalization for each mini-batch to accelerate network training [39]. In addition, *dropout* method [40] is adopted to prevent overfitting.

$$y = \frac{1}{1 + e^{-x}} \tag{10}$$

$$y = \max(0, x) \tag{11}$$

IV. EXPERIMENTAL RESULTS AND DISCUSSIONS

In this section, we comprehensively discuss the performance of proposed scheme. We first discuss the influence of sample

This article has been accepted for publication in a future issue of this journal, but has not been fully edited. Content may change prior to final publication. Citation information: DOI 10.1109/JLT.2020.2973232, Journal of Lightwave Technology

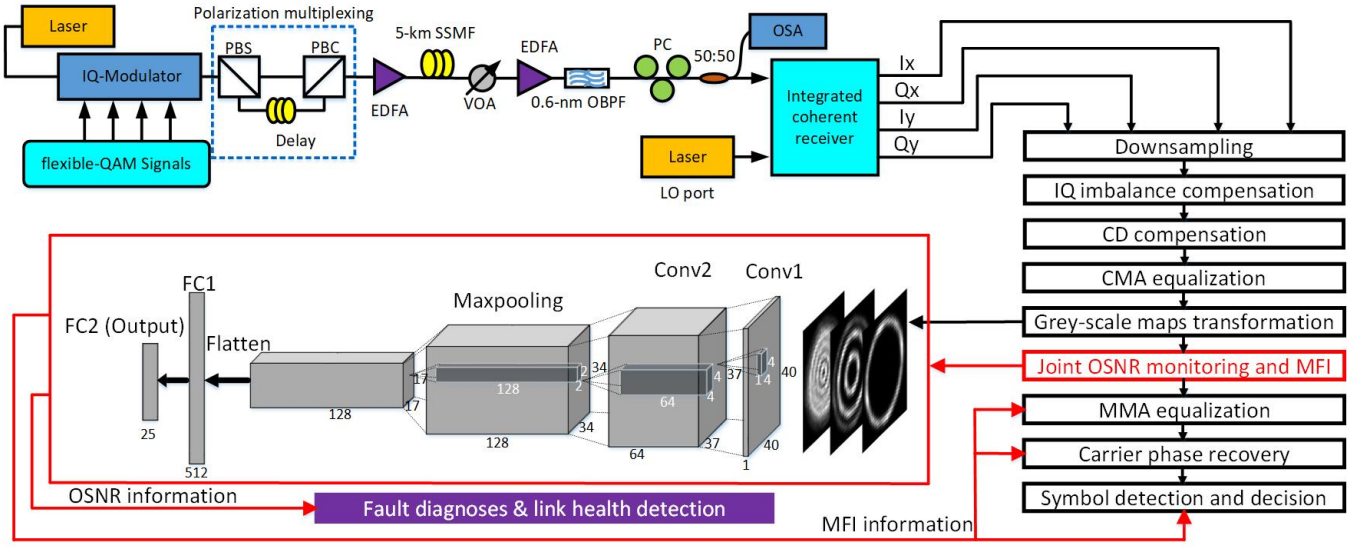

Fig. 3. Experimental setup for joint MFI and OSNR monitoring. PBS: polarization beam splitter; PBC: polarization beam combiner; EDFA: erbium-doped fiber amplifier; VOA: variable optical attenuator; OBPF: optical band-pass filter; PC: polarization controller; OSA: optical spectrum analyzer; LO: local oscillation; Conv: convolutional layer; FC: fully-connected layer.

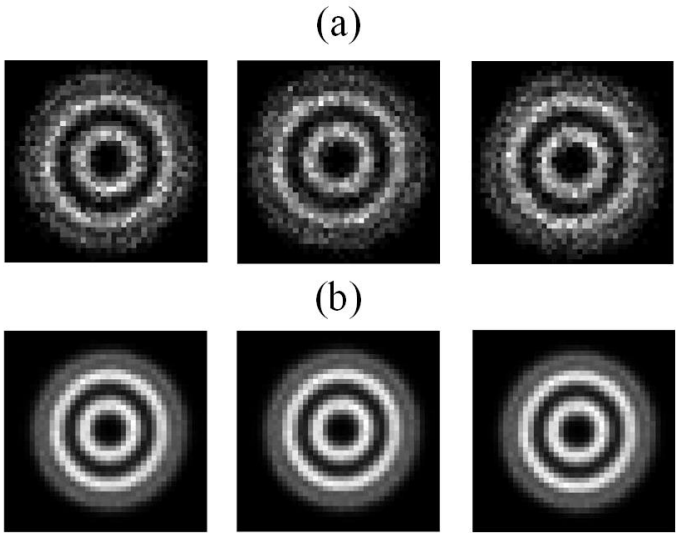

Fig. 4. Three different grayscale maps that is randomly selected from data sets with different value of L, (a) $L = 10^4$; (b) $L = 3 \times 10^5$.

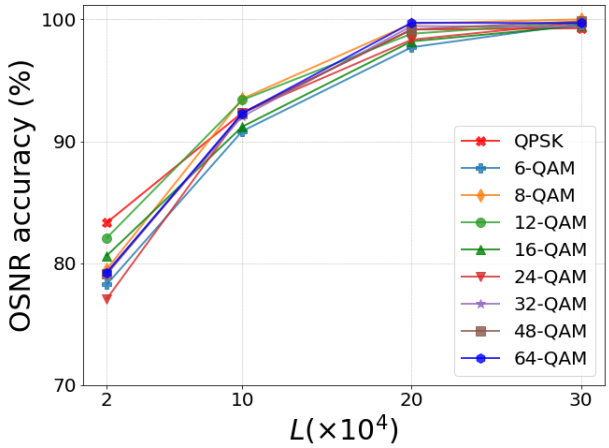

Fig. 5. OSNR accuracy vs. L.

length and resolution of grayscale maps in the data set. Then we compare the performance of B-CNN with F-CNN and MLP and discuss the advantages and disadvantages of B-CNN over the other two. Note that all the results below are the averaged results from five random weight initialization of DNNs.

A. Influence of sample length and resolution

In this section, we investigate how sample length (e.g. the length of time period in which we collect a grayscale map) and the resolution of a grayscale map influence the overall performance of joint MFI and OSNR monitoring. Hereafter we denote sample length by L and resolution by $R \times R$. As shown in Fig. 4, it is obvious that when L is small, the phase distribution of grayscale maps differ a lot from each other, which means that the difference within a category in the data set is large. On the other hand, when L is large, the phase distribution of grayscale maps are uniform, which indicates that the difference within a category in the data set is small. In other words, the boundary between different categories will be more apparent when L is large. Intuitively, since DNNs are discriminant models, the performance of DNNs will be better when L is larger. The results shown in Fig. 5 prove that the performance of B-CNN grows as L become larger.

Fig. 7 shows the performance of OSNR monitoring as a function of R. Since a grayscale map with higher resolution contains more information of the original signals as shown in Fig. 6, It is unsurprising that the accuracies of OSNR monitoring increase as R increase.

This article has been accepted for publication in a future issue of this journal, but has not been fully edited. Content may change prior to final publication. Citation information: DOI 10.1109/JLT.2020.2973232, Journal of Lightwave Technology

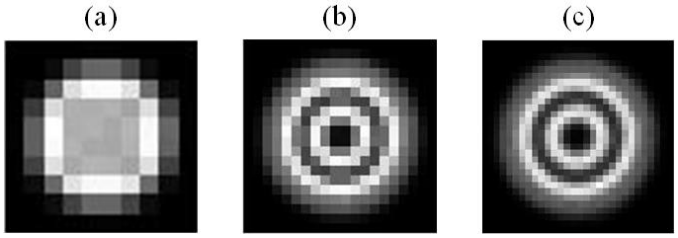

Fig. 6. Grayscale maps with different value of R, (a) $R = 10$; (b) $R = 20$; (c) $R = 30$.

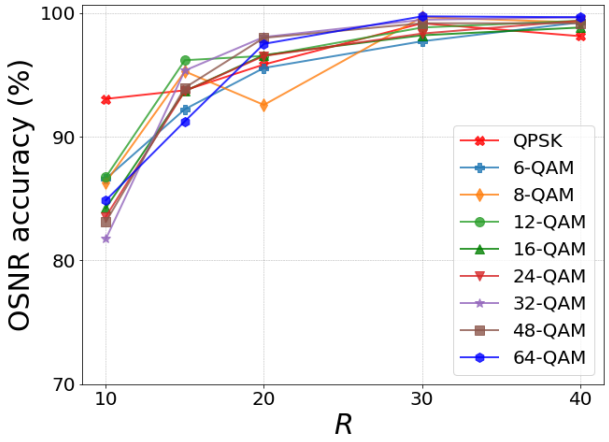

Fig. 7. OSNR accuracy vs. R.

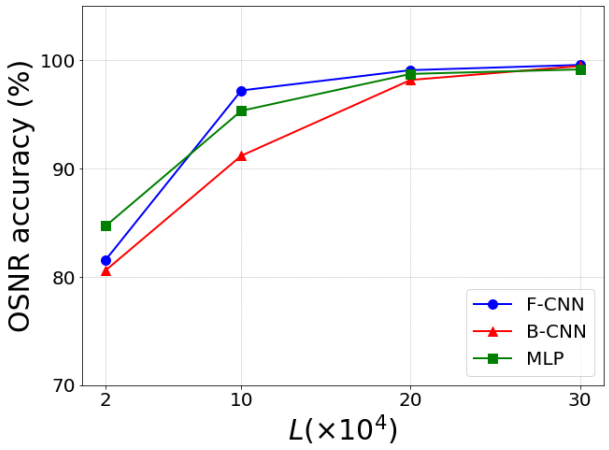

Fig. 8. OSNR accuracy of 16-QAM versus L for different DNNs, while R is fixed at 30.

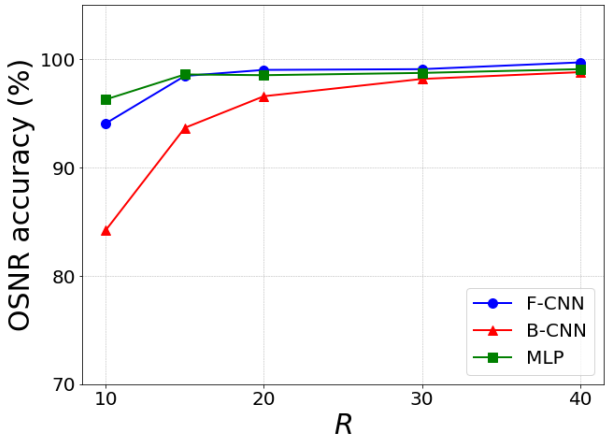

Fig. 9. OSNR accuracy of 16-QAM versus R for different DNNs, while L is fixed at 2×10^5.

B. Performance comparison between DNNs

Fig. 8, 9 shows the performance of OSNR monitoring using different DNNs as a function of L and R. For simplicity, we take the results for 16-QAM signals as an example. As depicted in Fig. 8, when R is fixed at 30, F-CNN and MLP can reach higher OSNR accuracy than B-CNN when $L < 2 \times 10^5$ and the performance of three DNNs are similar when $L \geq 2 \times 10^5$. Fig. 9 shows that when L is fixed at 2×10^5, the performance of F-CNN and MLP are better than B-CNN when $R < 30$ and the performance of three DNNs are similar when $R \geq 30$. Therefore, It can be concluded that MLP and F-CNN have higher tolerance of lower resolution and shorter sample length than B-CNN.

When we set the value of (L, R) at $(2 \times 10^5, 30)$, the performance of MFI and OSNR monitoring using different DNNs is depicted in Fig. 10. All three DNNs perform accurate MFI, both B-CNN and F-CNN reach 100% accuracy, while MLP reach 99.99%. The OSNR accuracy of B-CNN range from 97.71% to 99.72% with average accuracy of 98.91%, the OSNR accuracy of F-CNN range from 99.10% to 99.93% with average accuracy of 99.55%, and the range of MLP is from 97.15% to 99.86% with average value of 98.86%. According to the experimental results, we can conclude that F-CNN has the best performance, while B-CNN performs slightly worse than F-CNN but similarly to MLP. While the accuracies of predictions are generally similar between three DNNs, their memory consumption and execution speed in prediction are significantly different. We compute the memory size of each DNN when $(L, R) = (2 \times 10^5, 30)$ and compute the average execution time of each DNN from 20 times of forward propagation. As listed in Table II, B-CNN requires much lower memory consumption than F-CNN and MLP and reaches the fastest execution speed among three DNNs. This is due to the 1-bit weight and 1-bit wise arithmetic operation of BNNs, which has 32 times lower memory consumption and 23 times faster execution speed than floating points [35]. Therefore, we can conclude that B-CNN is more energy/time

This article has been accepted for publication in a future issue of this journal, but has not been fully edited. Content may change prior to final publication. Citation information: DOI 10.1109/JLT.2020.2973232, Journal of Lightwave Technology

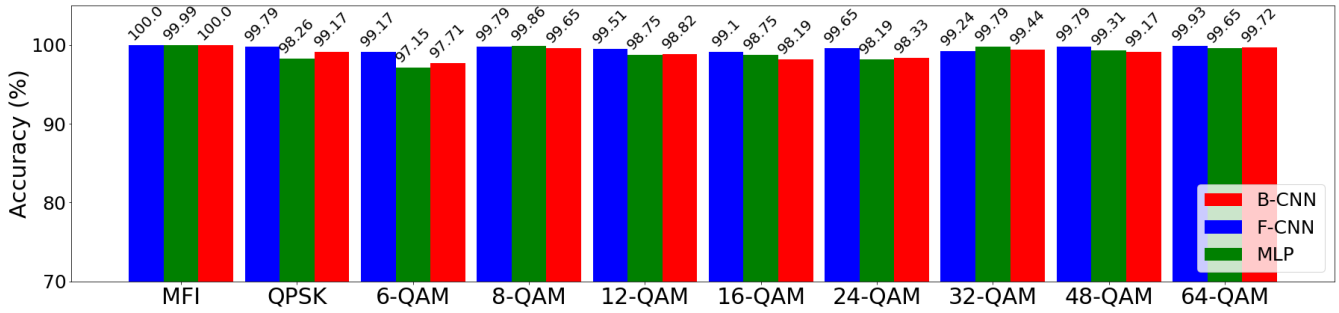

Fig. 10. Performance comparison of three DNNs, while $(L, R) = (2 \times 10^5, 30)$.

efficient than F-CNN and MLP

TABLE II
MEMORY SIZE AND EXECUTION SPEED OF DNNS

DNN type	F-CNN	MLP	B-CNN
Memory size (MB)	10.23	19.65	**3.13**
Execution time (s)	0.280	0.116	**0.059**

V. ROBUSTNESS EVALUATION

In future flexible optical networks, the transceivers will be reconfigurable and the physical parameters are changing. However, the data that we use in section IV is collected from the same link with fixed physical parameters, and it will be difficult and time consuming to train different models for different links. Therefore, we further evaluate the performance of proposed method when physical parameters are changing in a M-QAM simulation system.

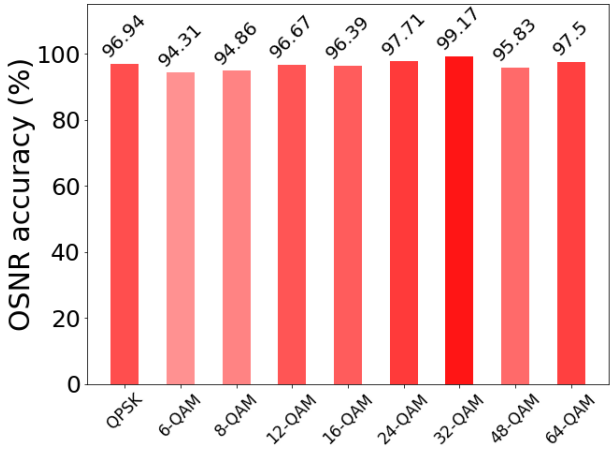

Fig. 11. Accuracy of OSNR estimation by B-CNN trained on data from three different distances (80 km, 160 km, and 240 km).

At first, we set the transmission distance at 80 km, 160 km and 240 km and evaluate the performance of B-CNN respectively. The value of (L, R) is set as $(2 \times 10^5, 40)$. Simulation results show that the accuracies of MFI and OSNR monitoring are all 100% for each transmission distance. Since the above

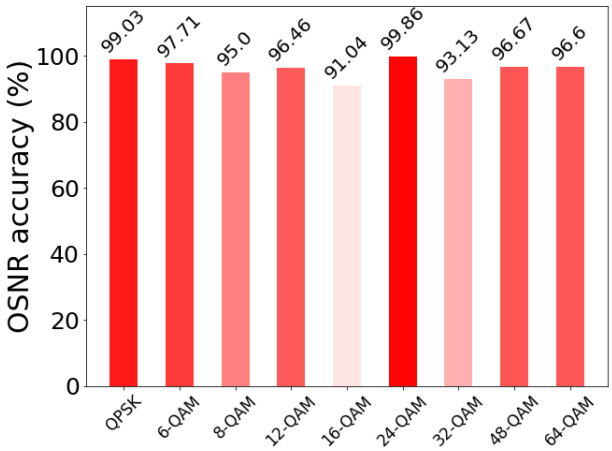

Fig. 12. Accuracy of OSNR estimation by B-CNN trained on data from three different launched powers (3 dBm, 5 dBm, and 7 dBm).

results are obtained by training B-CNN at different transmission distance respectively, we further explore the robustness of B-CNN to transmission distances by training it only once using all data from three different transmission distances. The accuracy of MFI remains 100%, which indicates that B-CNN is robust to transmission distance in MFI. The accuracies of OSNR estimation slightly decline as shown in Fig. 11. Next, we fix the transmission distance at 240 km and change the launched power to 3 dBm, 5 dBm and 7 dBm. The accuracies of MFI and OSNR monitoring are also 100% when we train the model separately. When we train B-CNN using all data from three different launched power, the performance is also reduced as shown in Fig. 12.

From the results above, we can conclude that B-CNN can reach high performance if we train it every time we change the physical parameters. However, when we use the data collected from a system with one changing parameter, the performance of B-CNN is reduced. In practical system with flexible transceivers, there may be more than one parameter that is dynamic. To further evaluate the performance of DNN-assisted OPM, we set up a simulation system with flexible configuration. Specifically, this system could be either dual-pol or single-pol, the transmission distance is set at 80 km, 160 km or 240 km, and the launched power is set at 3 dBm,

This article has been accepted for publication in a future issue of this journal, but has not been fully edited. Content may change prior to final publication. Citation information: DOI 10.1109/JLT.2020.2973232, Journal of Lightwave Technology

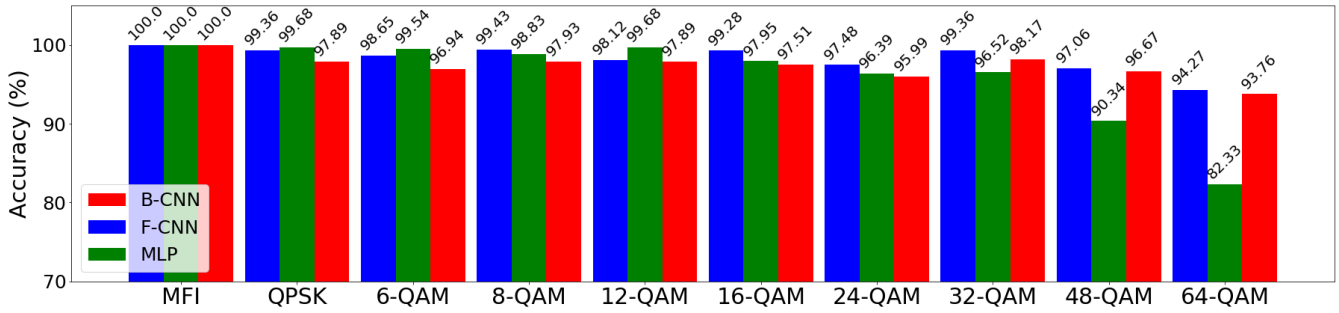

Fig. 13. Performance comparison of three DNNs trained upon composite date set.

5 dBm or 7 dBm. Therefore, the system has $2 \times 3 \times 3 = 18$ different parameter configurations. To reduce the training time, we collect 1440 grayscale maps for each system and hence the composite data set contains $1440 \times 18 = 25920$ samples in total.

Using the composite data set above, we train three different DNNs and the average accuracies are shown in Fig. 13. For MFI, all three DNNs reach 100% accuracy. Hence, in a system with dynamic parameters, MFI of DNN-assisted methods remain robust. On the other hand, the accuracies of OSNR monitoring are reduced by varying degree for different modulation formats and DNN types. For low-level QAM signals, F-CNN and MLP perform better than B-CNN. In contrast, F-CNN and B-CNN perform much better than MLP for high-level QAM signals including 32-QAM, 48-QAM and 64-QAM. In conclusion, CNNs are more robust in OSNR monitoring than MLP. Additionally, since binarization of CNN reduces its representation capacity, B-CNN has lower robustness than F-CNN. The results in this section motivate us to pursue further study in two directions. The first is to develop self-adaptive algorithms that are sensitive to the changing parameters. And the second is to explore new DNN-assisted method that has better trade-off in performance, robustness and complexity.

VI. Conclusion

In this paper, we have proposed and experimentally verified a joint OSNR monitoring and MFI technique in digital coherent receivers by processing ring constellations grayscale maps based on B-CNN. When the resolution of grayscale maps is set at 30×30 and the sample length is 2×10^5, the accuracy of MFI can reach 100% and the accuracies of OSNR monitoring can reach higher than 97.7% for nine M-QAM modulation formats. Compared with commonly used F-CNN and MLP, B-CNN can achieve the same MFI accuracy. For OSNR monitoring, the performance of B-CNN is slightly worse than that of F-CNN but similar to MLP. While the performances are similar among the three DNNs, B-CNN requires around 1/3 the memory consumption of F-CNN and 1/6 the memory consumption of MLP. In addition, the execution speed of B-CNN during forward propagation is fastest among the three DNNs. Therefore, B-CNN is most energy and time efficient compared with F-CNN and MLP and hence attractive for real-time OPM in future optical network.

References

[1] Y. Yin, K. Wen, D. J. Geisler, R. Liu, and S. Yoo, "Dynamic on-demand defragmentation in flexible bandwidth elastic optical networks," *Optics express*, vol. 20, no. 2, pp. 1798–1804, 2012.

[2] L. Gong and Z. Zhu, "Virtual optical network embedding (vone) over elastic optical networks," *Journal of Lightwave Technology*, vol. 32, no. 3, pp. 450–460, 2013.

[3] I. Tomkos, S. Azodolmolky, J. Sole-Pareta, D. Careglio, and E. Palkopoulou, "A tutorial on the flexible optical networking paradigm: State of the art, trends, and research challenges," *Proceedings of the IEEE*, vol. 102, no. 9, pp. 1317–1337, 2014.

[4] H. Khodakarami, B. S. G. Pillai, B. Sedighi, and W. Shieh, "Flexible optical networks: An energy efficiency perspective," *Journal of Lightwave Technology*, vol. 32, no. 21, pp. 3356–3367, 2014.

[5] D. Klonidis, F. Cugini, O. Gerstel, M. Jinno, V. Lopez, E. Palkopoulou, M. Sekiya, D. Siracusa, G. Thouénon, and C. Betoule, "Spectrally and spatially flexible optical network planning and operations," *IEEE Communications Magazine*, vol. 53, no. 2, pp. 69–78, 2015.

[6] G. S. Zervas and D. Simeonidou, "Cognitive optical networks: Need, requirements and architecture," in *2010 12th International Conference on Transparent Optical Networks*. IEEE, 2010, pp. 1–4.

[7] W. Wei, C. Wang, and J. Yu, "Cognitive optical networks: Key drivers, enabling techniques, and adaptive bandwidth services," *IEEE Communications magazine*, vol. 50, no. 1, pp. 106–113, 2012.

[8] I. De Miguel, R. J. Durán, T. Jiménez, N. Fernández, J. C. Aguado, R. M. Lorenzo, A. Caballero, I. T. Monroy, Y. Ye, A. Tymecki *et al.*, "Cognitive dynamic optical networks," *Journal of Optical Communications and Networking*, vol. 5, no. 10, pp. A107–A118, 2013.

[9] R. Borkowski, R. J. Durán, C. Kachris, D. Siracusa, A. Caballero, N. Fernández, D. Klonidis, A. Francescon, T. Jiménez, J. C. Aguado *et al.*, "Cognitive optical network testbed: Eu project chron," *Journal of Optical Communications and Networking*, vol. 7, no. 2, pp. A344–A355, 2015.

[10] A. E. Willner, Z. Pan, and C. Yu, "Optical performance monitoring," in *Optical Fiber Telecommunications VB*. Elsevier, 2008, pp. 233–292.

[11] F. N. Hauske, M. Kuschnerov, B. Spinnler, and B. Lankl, "Optical performance monitoring in digital coherent receivers," *Journal of Lightwave Technology*, vol. 27, no. 16, pp. 3623–3631, 2009.

[12] C. C. Chan, *Optical performance monitoring: advanced techniques for next-generation photonic networks*. Academic Press, 2010.

[13] Z. Dong, F. N. Khan, Q. Sui, K. Zhong, C. Lu, and A. P. T. Lau, "Optical performance monitoring: A review of current and future technologies," *Journal of Lightwave Technology*, vol. 34, no. 2, pp. 525–543, 2015.

[14] M. A. Jarajreh, E. Giacoumidis, I. Aldaya, S. T. Le, A. Tsokanos, Z. Ghassemlooy, and N. J. Doran, "Artificial neural network nonlinear equalizer for coherent optical ofdm," *IEEE Photonics Technology Letters*, vol. 27, no. 4, pp. 387–390, 2014.

[15] J. Thrane, J. Wass, M. Piels, J. C. Diniz, R. Jones, and D. Zibar, "Machine learning techniques for optical performance monitoring from directly detected pdm-qam signals," *Journal of Lightwave Technology*, vol. 35, no. 4, pp. 868–875, 2016.

[16] B. Karanov, M. Chagnon, F. Thouin, T. A. Eriksson, H. Bülow, D. Lavery, P. Bayvel, and L. Schmalen, "End-to-end deep learning of optical fiber communications," *Journal of Lightwave Technology*, vol. 36, no. 20, pp. 4843–4855, 2018.

[17] T. Tanimura, T. Hoshida, T. Kato, S. Watanabe, and H. Morikawa, "Convolutional neural network-based optical performance monitoring

for optical transport networks," *Journal of Optical Communications and Networking*, vol. 11, no. 1, pp. A52–A59, 2019.

[18] F. N. Khan, K. Zhong, X. Zhou, W. H. Al-Arashi, C. Yu, C. Lu, and A. P. T. Lau, "Joint osnr monitoring and modulation format identification in digital coherent receivers using deep neural networks," *Optics express*, vol. 25, no. 15, pp. 17 767–17 776, 2017.

[19] D. Wang, M. Zhang, J. Li, Z. Li, J. Li, C. Song, and X. Chen, "Intelligent constellation diagram analyzer using convolutional neural network-based deep learning," *Optics express*, vol. 25, no. 15, pp. 17 150–17 166, 2017.

[20] X. Fan, Y. Xie, F. Ren, Y. Zhang, X. Huang, W. Chen, T. Zhangsun, and J. Wang, "Joint optical performance monitoring and modulation format/bit-rate identification by cnn-based multi-task learning," *IEEE Photonics Journal*, vol. 10, no. 5, pp. 1–12, 2018.

[21] J. Zhang, W. Chen, M. Gao, Y. Ma, Y. Zhao, and G. Shen, "Intelligent adaptive coherent optical receiver based on convolutional neural network and clustering algorithm," *Optics express*, vol. 26, no. 14, pp. 18 684–18 698, 2018.

[22] Z. Wan, Z. Yu, L. Shu, Y. Zhao, H. Zhang, and K. Xu, "Intelligent optical performance monitor using multi-task learning based artificial neural network," *Optics express*, vol. 27, no. 8, pp. 11 281–11 291, 2019.

[23] Y. Cheng, S. Fu, M. Tang, and D. Liu, "Multi-task deep neural network (mt-dnn) enabled optical performance monitoring from directly detected pdm-qam signals," *Optics Express*, vol. 27, no. 13, pp. 19 062–19 074, 2019.

[24] D. Wang, M. Wang, M. Zhang, Z. Zhang, H. Yang, J. Li, J. Li, and X. Chen, "Cost-effective and data size–adaptive opm at intermediated node using convolutional neural network-based image processor," *Optics Express*, vol. 27, no. 7, pp. 9403–9419, 2019.

[25] Z. Yu, Z. Wan, L. Shu, S. Hu, Y. Zhao, J. Zhang, and K. Xu, "Loss weight adaptive multi-task learning based optical performance monitor for multiple parameters estimation," *Optics Express*, vol. 27, no. 25, pp. 37 041–37 055, 2019.

[26] R. Borkowski, D. Zibar, A. Caballero, V. Arlunno, and I. T. Monroy, "Optical modulation format recognition in stokes space for digital coherent receivers," in *Optical Fiber Communication Conference*. Optical Society of America, 2013, pp. OTh3B–3.

[27] J. Liu, Z. Dong, K. Zhong, A. P. T. Lau, C. Lu, and Y. Lu, "Modulation format identification based on received signal power distributions for digital coherent receivers," in *Optical Fiber Communication Conference*. Optical Society of America, 2014, pp. Th4D–3.

[28] S. M. Bilal, G. Bosco, Z. Dong, A. P. T. Lau, and C. Lu, "Blind modulation format identification for digital coherent receivers," *Optics express*, vol. 23, no. 20, pp. 26 769–26 778, 2015.

[29] M. Xiang, Q. Zhuge, M. Qiu, X. Zhou, M. Tang, D. Liu, S. Fu, and D. V. Plant, "Rf-pilot aided modulation format identification for hitless coherent transceiver," *Optics express*, vol. 25, no. 1, pp. 463–471, 2017.

[30] R. Schmogrow, B. Nebendahl, M. Winter, A. Josten, D. Hillerkuss, S. Koenig, J. Meyer, M. Dreschmann, M. Huebner, C. Koos *et al.*, "Error vector magnitude as a performance measure for advanced modulation formats," *IEEE Photonics Technology Letters*, vol. 24, no. 1, pp. 61–63, 2011.

[31] M. S. Faruk, Y. Mori, and K. Kikuchi, "In-band estimation of optical signal-to-noise ratio from equalized signals in digital coherent receivers," *IEEE Photonics Journal*, vol. 6, no. 1, pp. 1–9, 2014.

[32] M. R. Chitgarha, S. Khaleghi, W. Daab, A. Almaiman, M. Ziyadi, A. Mohajerin-Ariaei, D. Rogawski, M. Tur, J. D. Touch, V. Vusirikala *et al.*, "Demonstration of in-service wavelength division multiplexing optical-signal-to-noise ratio performance monitoring and operating guidelines for coherent data channels with different modulation formats and various baud rates," *Optics letters*, vol. 39, no. 6, pp. 1605–1608, 2014.

[33] L. Lundberg, H. Sunnerud, and P. Johannisson, "In-band osnr monitoring of pm-qpsk using the stokes parameters," in *Optical Fiber Communication Conference*. Optical Society of America, 2015, pp. W4D–5.

[34] A. Coates, B. Huval, T. Wang, D. Wu, B. Catanzaro, and N. Andrew, "Deep learning with cots hpc systems," in *International conference on machine learning*, 2013, pp. 1337–1345.

[35] M. Courbariaux, I. Hubara, D. Soudry, R. El-Yaniv, and Y. Bengio, "Binarized neural networks: Training deep neural networks with weights and activations constrained to+ 1 or-1," *arXiv preprint arXiv:1602.02830*, 2016.

[36] A. T. Le and K. Araki, "A group of modulation schemes for adaptive modulation," in *2008 11th IEEE Singapore International Conference on Communication Systems*. IEEE, 2008, pp. 864–869.

[37] A. Gulli and S. Pal, *Deep Learning with Keras*. Packt Publishing Ltd, 2017.

[38] D. P. Kingma and J. Ba, "Adam: A method for stochastic optimization," *arXiv preprint arXiv:1412.6980*, 2014.

[39] S. Ioffe and C. Szegedy, "Batch normalization: Accelerating deep network training by reducing internal covariate shift," *arXiv preprint arXiv:1502.03167*, 2015.

[40] N. Srivastava, G. Hinton, A. Krizhevsky, I. Sutskever, and R. Salakhutdinov, "Dropout: a simple way to prevent neural networks from overfitting," *The journal of machine learning research*, vol. 15, no. 1, pp. 1929–1958, 2014.